atmosphere

MDPI

Article

The Synthesis of $FeCl_3$-Modified Char from Phoenix Tree Fruit and Its Application for Hg^0 Adsorption in Flue Gas

Wei Chen [1,†], Ming Li [2,†], Zirui Hu [1] and Chong Tian [1,*]

[1] Power and Mechanical Engineering, Wuhan University, Wuhan 430072, China; 2020202080046@whu.edu.cn (W.C.); 2019302080228@whu.edu.cn (Z.H.)
[2] School of Energy and Power Engineering, Wuhan University of Technology, Wuhan 430070, China; lm825640619@whut.edu.cn
* Correspondence: ctian@whu.edu.cn
† These authors contributed equally to this work.

Abstract: A sample of $FeCl_3$-modified phoenix tree fruit char (MPTFC) was prepared using pyrolysis and a facile chemical immersion method; it was proposed as an effective sorbent for Hg^0 adsorption in flue gas. The BET, SEM, FTIR, and XPS methods were adopted for the characterizations of the sorbents, and a series of Hg^0 adsorption tests were conducted on a bench-scale Hg^0 removal setup in the lab. The morphological analysis of the sorbent indicated that the hollow fiber in phoenix tree fruit (PTF) shifted to organized directional porous tubular columns in phoenix tree fruit char (PTFC) after pyrolysis. The surface area of MPTFC increased slightly in comparison with PTF and PTFC. The MPTFC showed excellent performance for Hg^0 adsorption at 200 °C in flue gas ambiance, and the Hg^0 removal efficiency approached 95% with 5% (wt.%) $FeCl_3$ modification. The presence of O_2 may help to activate the MPTFC for Hg^0 adsorption in flue gas, thus greatly promoting Hg^0 adsorption capability. NO had a positive effect on Hg^0 adsorption, while the presence of SO_2 in flue gas restrained Hg^0 adsorption by MPTFC. Functional groups, such as C-Cl and Fe-O, were successfully decorated on the surface of PTFC by $FeCl_3$ modification, which contributed greatly to Hg^0 adsorption. In addition, C=O, lattice oxygen (O_α), and adsorbed oxygen (O_β) also contributed to Hg^0 adsorption and oxidization.

Keywords: phoenix tree fruit; modified bio-char; Hg^0 removal; flue gas

Citation: Chen, W.; Li, M.; Hu, Z.; Tian, C. The Synthesis of $FeCl_3$-Modified Char from Phoenix Tree Fruit and Its Application for Hg^0 Adsorption in Flue Gas. *Atmosphere* **2022**, *13*, 1093. https://doi.org/10.3390/atmos13071093

Academic Editors: Christoffer Boman and Kumar Vikrant

Received: 6 June 2022
Accepted: 8 July 2022
Published: 11 July 2022

1. Introduction

Mercury (Hg) in the atmosphere is characterized by hypertoxicity, bioaccumulation, and persistence; it is detrimental to both the environment and public health worldwide [1–3]. Most of the Hg in the ecosystem originates from human activities, and it is important to control anthropogenic Hg emissions. Coal-fired power plants are considered to be one of the major emission sources of Hg in the atmosphere [4]. To reduce Hg emissions from coal-fired electricity generation, the strictest emission limitations (GB13223-2011) in the world have been announced and put into practice by the Chinese Environmental Ministry. Besides the standards set for conventional sources of pollution, such as PMs, SO_2, and NO, clear emission limitations have also been issued, for the first time, for pollution caused by non-conventional heavy metals such as Hg. Recently, a stricter standard with a maximum Hg emission concentration of 1 $\mu g/m^3$ was proposed for abating Hg emissions from coal-fired power plants [5,6]. Herein, we state that controlling Hg emissions from coal-fired electricity generation is an urgent and significant issue.

Although Hg is present in coal in trace amounts, the total emissions are nevertheless very significant because of the heavy and long-term use of coal as the major source of energy in China [7–10]. Hg first evaporates as Hg^0 vapor during coal combustion; then, a series of chemical reactions occur over a wide range of temperature drops in the flue gas. Hg releases

into the atmosphere as three major species, namely Hg^0, Hg^{2+}, and Hg^P. Hg^{2+} is easily dissolved in water; thus, it is removed by wet flue gas desulfurization (WFGD) systems. Hg^P is captured by electrostatic precipitators (ESPs) together with particles. However, Hg^0 is hard to remove because of its chemical stability. Therefore, the removal of Hg^0 from flue gas is an important problem that poses several difficulties [11,12].

The use of sorbents for the post-combustion removal of Hg^0 from flue gas is one promising technology. Many sorbents have been developed for Hg^0 adsorption, including carbon-based and non-carbon sorbents [13]. Carbon-based materials, such as activated carbon, show a strong Hg^0 adsorption capability. Hg^0 is adsorbed on the surface of carbon-based sorbents by surface reactions among Hg^0 and surface functional groups. Functional groups that include oxygen, halogens, sulfur, and active metal agents can be functionalized on the surface of the sorbents, enhancing the capability for Hg^0 adsorption [14–18]. Activated carbon (AC) has also been adopted for use in Hg^0 removal in industrial applications worldwide. However, one of the disadvantages of AC is its high cost for large-scale commercial applications. Therefore, developing low-cost carbon-based sorbents for Hg^0 adsorption is essential [19–21].

Biomass, which is abundant and easily obtained in nature, is one of the promising candidates for use as a carbon-based substrate for Hg^0 adsorption [22,23]. Research has been conducted on modified sargassum chars, waste tea char, seaweed chars, and modified bamboo char to investigate their Hg^0 adsorption capabilities [24–29]. However, some chars prepared from biomass possess undeveloped pore structures, which result in poor chemical kinetics and mass transfer performance, thus limiting the diffusion of Hg^0 in the sorbents. In addition, some of the surface functional groups on the char may break away from the sorbents at high temperatures, thus decreasing Hg^0 adsorption capacity.

Phoenix tree fruit (PTF), which is common and abundant in cities all over the world, is the fruit of the French sycamore. The flocculant of the PTF is fiber-shaped with pores, suggesting its potential adsorption capability. The hollow fiber microstructures may be helpful for mass transfer and diffusion, thus promoting the adsorption capability of PTF. However, PTF is not well utilized as a biomass source. For the first time, we use PTF as the raw biomass material to develop a carbon-based material with porous structures for Hg^0 adsorption. In this work, we report the properties of $FeCl_3$-modified phoenix tree fruit char (MPTFC) and its capability for Hg^0 adsorption. The effects of temperature and the flue gas components on the performance of Hg^0 adsorption are also thoroughly presented. We hope to establish a possible pathway for the utilization of PTF for Hg^0 reduction in industrial applications.

2. Materials and Methods

2.1. Char Preparation from Phoenix Tree Fruit and $FeCl_3$ Modification

First, the char (PTFC) was prepared by pyrolysis from phoenix tree fruit (PTF) in an N_2 atmosphere at a flow rate of 300 mL/min for 30 min at 600 °C. After that, the phoenix tree fruit char (PTFC) was then modified with $FeCl_3$ by a facile chemical immersion method in solutions with different concentrations of $FeCl_3$. Solid $FeCl_3$ was first diluted in DI water to produce $FeCl_3$-containing solutions with weight percentages of 1%, 3%, 5%, and 7%. Then, 1 g PTFC was mixed with 3 mL of each of the $FeCl_3$ solutions of different concentrations in a beaker with magnetic stirring for 60 min. Then, the mixture system was ultrasound shocked for 10 min. After that, the mixtures were filtered and transferred to an oven to dry at 105 °C for 12 h. The modified PTFC (MPTFC) was obtained.

2.2. Analytical Methods

Several characterization methods, namely BET, SEM, EDS, FTIR, and XPS, were adopted for the characterization of MPTFC. The specific area (BET) analysis was adopted for measuring the surface area of the sorbents, and the BET analysis was conducted using the Micrometrics TriStar II 3020 from the United States of America. The SEM analysis method was used for micro-morphology observations, and the tests were conducted on

the QUANTA200 from the FEI company at Wuhan University. In addition, the energy dispersive spectrometer (EDS) method was used to identify the elemental distributions in the sorbents in order to confirm the success of the Fe–Cl impregnations. The EDS analysis was conducted using the Horiba 7021-H. Further, the Nicolet 6700 Fourier transform infrared (FTIR) spectrometer was adopted to identify the molecular surface structure and the functional groups on the surface of the sorbents. The FTIR measurements were conducted at Wuhan University. In addition, X-ray photoelectron spectroscopy (XPS) was used for elemental valence state characterizations on the surface of the sorbents. The XPS equipment we used in the experiments was the G2f20 from TECNAI; the reference calibration junction energy was 284.6 eV, and the error was ±0.3 eV.

2.3. Hg Adsorption Experiments

The Hg^0 removal setup is shown in Figure 1. The experimental system can be divided into five major parts, namely the gas feeding and mixture system, the Hg^0 generation system, the main reaction system, the Hg^0 monitoring system, and the exhaust purification system.

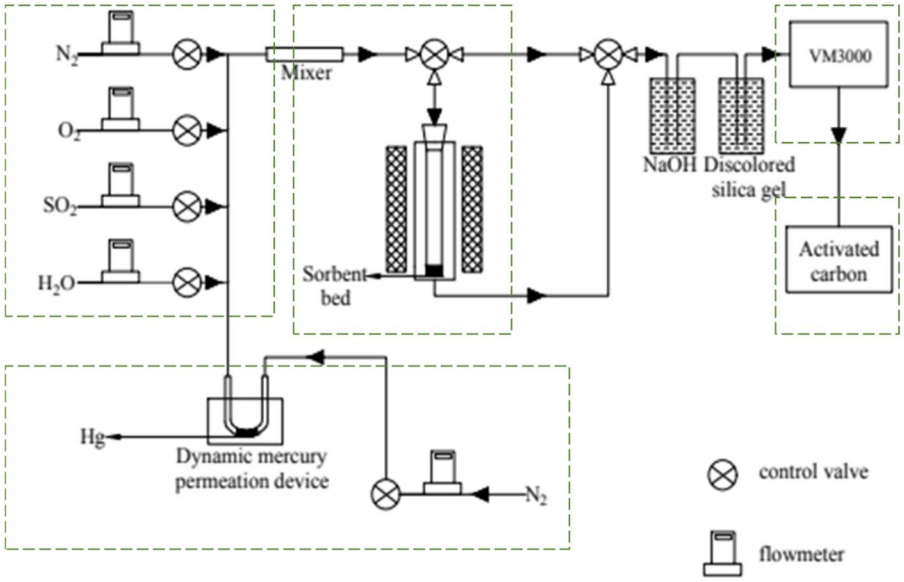

Figure 1. Bench-scale experimental system for Hg^0 adsorption.

The gas feeding system chiefly consisted of sources of O_2, N_2, NO, and SO_2 with a mass flow controller for control of the flow rate. The simulated flue gas was mostly composed of the 4 gases listed above, with proportions chosen to simulate the components of flue gas. The Hg^0 generation system used a Dynacalibrator Model 500 mercury penetration tube. The steady Hg^0 generation system also consisted of a water bath, N_2 as a carrier gas with a flow rate of 300 mL/min, a U-shaped tube for Hg^0 penetration, and a tube holder. The initial Hg^0 concentration was maintained at 50μg/m^3 by controlling the temperature of the water bath at 60 °C. The main part of the adsorption reaction system was a vertical fixed bed, which mainly consisted of an electric furnace and an annular quartz tube reactor. The diameter of the inner tube was 14 mm with a quartz sieve plate. During the reactions, the sorbents were placed in the plate covered by quartz wool to inhibit the blowing of the sorbent during gas feeding. During the experiment, the Hg^0 vapor passed through the sorbents, and the Hg^0 adsorption reactions occurred in the gas–solid reaction system. A VM3000 from Mercury Instruments in Germany was used for Hg^0 online monitoring, and the detection precision was about 0.1 μg/m^3. The exhaust first passed through activated carbon to dispose of the remaining Hg^0 before it was sucked into a vent.

A series of experiments were conducted, and the detailed experimental arrangements are as listed in Table 1. The Hg^0 removal efficiency η is calculated by using the following Equation (1):

$$\eta = 1 - \frac{C_t}{C_0} \times 100\% \quad (1)$$

where η is the Hg^0 removal efficiency; C_t and C_0 stand for the Hg^0 concentration at t seconds and the initial Hg^0 concentration, respectively.

Table 1. Hg^0 adsorption experiments on MPTFCs.

No. \ Conditions	Gas Components	Total Gas Flow Rate (L/mol)	Initial Hg^0 Concentration (μg/m^3)	Reaction Temperature (°C)	Sorbent Mass (mg)
1	8% O_2, N_2	1	50	200	100
2	8% O_2, N_2	1	50	150/200/250/300	100
3	N_2	1	50	100/150/200/250/300	100
4	8% O_2, N_2 500 ppm SO_2 0~700 ppm NO	1	50	200	100
5	8% O_2, N_2 0~1500 ppm SO_2 200 ppm NO	1	50	200	100
6	8% O_2, N_2	1	50	200	100

3. Results and Discussions

3.1. Properties of the Phoenix Tree Fruit

The proximate and ultimate analyses of PTF are shown in Table 2. It can be observed that the major components are volatiles (72.08%) and fixed carbon (15.93%). However, the moisture and ash contents are relatively low, only accounting for 5.41% and 6.58%, respectively. The high content of volatiles in the materials was the basis for concluding that a flourishing porous structure would result when the char was prepared by pyrolysis; this would enhance adsorption capability. The major elements in PTF are C and O, at around 66% and 35%, respectively. Meanwhile, the contents of H, N, and S are relatively low. The abundance of C and O in PTF creates more chances to form oxygen-containing functional groups during pyrolysis. Those oxygen-containing groups are believed to benefit the promotion of Hg^0 adsorption capability. Meanwhile, the lower contents of N and S reduce the possibility of N- and S-bearing gas emissions during pyrolysis, thus reducing the potential environmental pollution caused by pyrolysis.

Table 2. Proximate and ultimate analyses of the phoenix tree fruit.

Sample	Proximate Analysis (wt.%, Dry Basis)					Ultimate Analysis (wt.%, Dry and Ash-Free Basis)			
	C^{daf}	H^{daf}	O^{daf}	N^{daf}	S^{t}	M^{ad}	V^{daf}	A^{d}	FC^{daf}
PTF	65.98	3.42	34.74	1.86	0.52	5.41	72.08	6.58	15.93

M: moisture; V: volatile; A: ash; FC: fixed carbon; S^{t}: total sulfur; daf: dry and ash-free basis; ad: air-dried; d: dry basis.

3.2. SEM Observations

The SEM observations for PTF, PTFC, and MPTFC are shown in Figure 2. It can be seen that the original PTF has a hollow fiber shape with compact layer structures, and the diameter of the fiber is about 20 μm. Both the surface and the inner layer of the fiber seem to be smooth and without pores. However, the micro-morphology of PTFC is very different in comparison to that of PTF. The hollow fiber shape shifts to organized directional tubular columns. A single tubular structure is about 10 μm in diameter, while the column is about 50 μm in diameter. Some cracks and pores can also be observed on the surface of the tubular

structure. Those alterations in morphology are highly suspected to result from the release of volatiles during pyrolysis. The violent gas explosion from the inside of the PTF caused the expansion of the layer structures, thus producing the organized tubular columns. Those changes benefited PTFC in terms of adsorption because of the relatively higher number of porous structures. The micro-morphology of MPTFC is almost the same as that of PTFC, which indicates that the $FeCl_3$ modifications only functionalized the surface of the material.

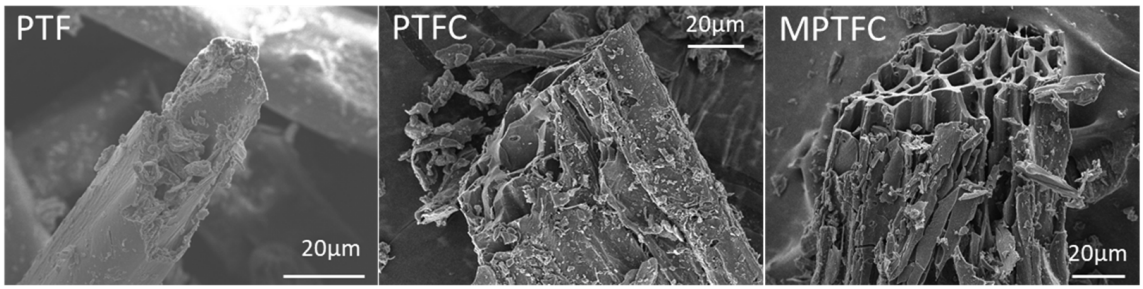

Figure 2. SEM observations of the sorbents.

3.3. BET Analysis of the Sorbents

The BET(BET surface area, SBET, m^2/g) analysis results are shown in Table 3. The results reveal that the surface area of PTF is around 2.4 m^2/g, and the surface area of PTFC is around 3.4 m^2/g. The increase in the surface area from PTF to PTFC is highly suspected to be linked to the volatilization of the volatile matter, including CO_2 and H_2O. The release of those gas components produces porous structures, thus increasing the surface area. However, the surface area of MPTFC is larger in comparison with PTF and PTFC. The concentrations of the precursor also have some impact on the surface area. When the concentration of $FeCl_3$ increased from 3% (wt.%) to 5% (wt.%), the surface area increased from 5.8 m^2/g to 10.6 m^2/g. However, when the concentration increased to 7% (wt.%), the surface area decreased slightly to 8.4 m^2/g; this is highly suspected to be linked to the blocking of the pores and tubular channels by the higher concentration of the Fe–Cl precursor.

Table 3. Surface area of the sorbents (m^2/g).

Sample	PTF	PTFC	MPTFC-3	MPTFC-5	MPTFC-7
Surface area	2.4	3.4	5.8	10.6	8.4

3.4. Hg^0 Adsorption Performance

3.4.1. Effects of Temperature on Hg^0 Removal by PTFC

To evaluate the effects of temperature on the performance efficiency of PTFC for Hg^0 removal, we conducted the Hg^0 adsorption experiments at different temperatures in the N_2 ambiance. The Hg^0 removal efficiencies as a function of temperature are shown in Figure 3. It can be seen that the optimal temperature for Hg^0 adsorption by PTFC was 150 °C; the efficiency was greater than 50%. As the temperature increased, the Hg^0 removal efficiency of PTFC decreased, falling to 16% when the temperature increased to 300 °C. The results indicate that physical adsorption may dominate the Hg^0 adsorption of PTFC in N_2 +8% O_2 ambiance. Hg^0 was physically adsorbed on the surface of the PTFC and then diffused in the tubular columns in the gas flow fields. The binding force between the Hg^0 and the PTFC was weak, thus, it was desorbed as temperature increased as a result of the intensification of molecular motion.

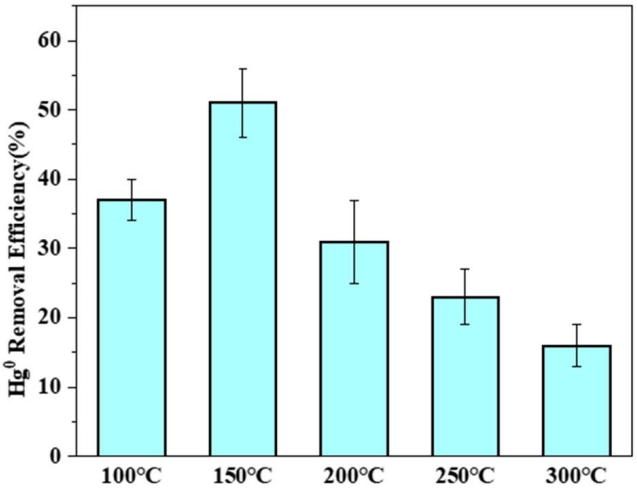

Figure 3. Hg^0 removal efficiency of PTFC as a function of temperature.

3.4.2. Effects of Temperature on Hg^0 Removal by MPTFC

The Hg^0 adsorption capabilities of MPTFC as a function of temperature are shown in Figure 4. It can be seen that $FeCl_3$ modification of PTFC can greatly promote Hg^0 adsorption capability in comparison with PTFC. However, temperature also has an impact on MPTFC's efficacy for Hg^0 removal. Its Hg^0 removal efficiency increased from 73% to 95% when the temperature increased from 150 °C to 200 °C, respectively. However, the Hg^0 removal efficiency decreased to 83% and 74% when the temperature continued increasing to 250 °C and 300 °C, respectively. It can be concluded that the optimal temperature for Hg^0 adsorption by MPTFC is 200 °C, which is slightly different from that of PTFC. It can be inferred that the Hg^0 adsorption mechanisms are different for PTFC and MPTFC. Regarding PTFC, Hg^0 physical adsorption on the surface of the sorbent is more likely to be the dominating reaction. However, high temperature intensifies molecular thermal motion, thus weakening the surface force of Hg^0 adsorption by PTFC [30,31]. However, when the Fe–Cl functional groups are introduced on the surface of the sorbent, both physical and chemical adsorption reactions occur. The increase in temperature in a certain range promotes chemisorption reactions, thus enhancing the Hg^0 adsorption capability.

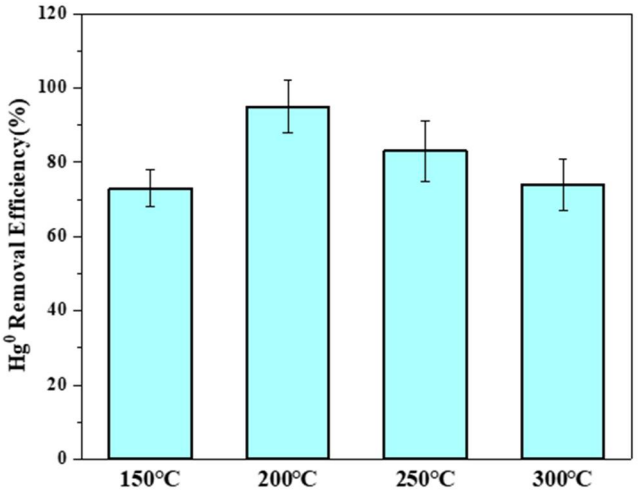

Figure 4. Effects of temperature on the Hg^0 removal capability of MPTFC.

3.4.3. Effects of $FeCl_3$ Concentrations on MPTFC for Hg^0 Removal

The $FeCl_3$ precursor we used for the PTFC modifications was prepared in a concentration gradient from 1% (wt.%) to 7% (wt.%) with intervals of 2% (wt.%). The series of MPTFCs with different levels of $FeCl_3$ modifications was tested for Hg^0 adsorption capability at 200 °C in N_2 + 8%O_2 ambiance. The Hg^0 removal efficiencies for all MPTFCs are shown in Figure 5.

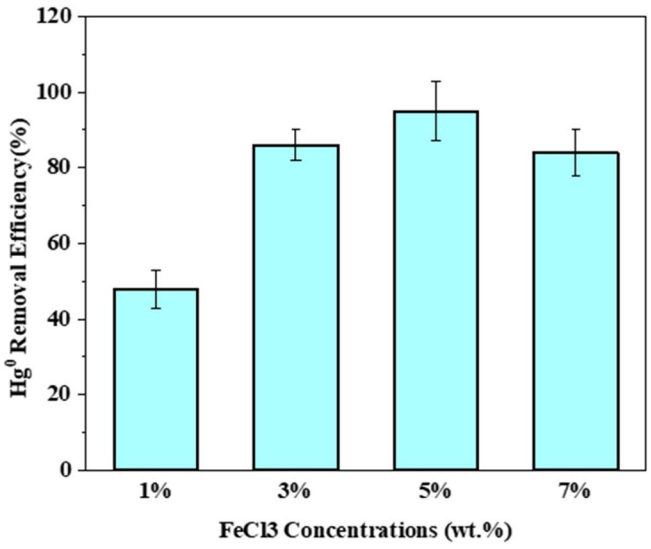

Figure 5. Hg^0 adsorption by MPTFCs with different concentrations of $FeCl_3$ as a precursor.

The introduction of $FeCl_3$ to PTFC can help promote Hg^0 adsorption capability. The Hg^0 removal capabilities of MPTFC showed an increasing trend with increasing concentrations of $FeCl_3$ from 1% (wt.%) to 5% (wt.%). The corresponding Hg^0 removal efficiencies increased from 48% to 95%. However, Hg^0 removal efficiency decreased to 84% when the $FeCl_3$ concentration continued increasing to 7% (wt.%). This result indicates that the most optimal concentration of $FeCl_3$ as a precursor for PTFC modification was 5% (wt.%). It can be seen that the presence of Fe^{3+} and Cl^- had positive consequences for Hg^0 oxidization, thus enhancing the chemisorption reactions for Hg^0 on the surface. Fe^{3+} has a strong oxidization capability in reactions, while Cl^- is easy to complex with Hg-containing compounds, thus causing Hg^0 oxidization in the reaction. In addition, the modification of PTFC with $FeCl_3$ also enlarged the surface area of the sorbents, which contributed to Hg^0 removal. The BET analysis also indicated that the surface area of MPTFC with the 5% $FeCl_3$ pretreatment was the highest in comparison with the other MPTFCs.

3.4.4. Effects of O_2 on Hg^0 Removal by the Sorbents

Here, we discuss the effects of the presence of O_2 on the adsorption capabilities of MPTFC. The MPTFC modified with 5% $FeCl_3$ was tested for its Hg^0 adsorption capability in N_2 ambiance at different temperatures. The results are shown in Figure 6. It can be observed that MPTFC did not perform as well as in the ambiance containing O_2. The Hg^0 removal efficiency decreased significantly in comparison with that observed in the 8% O_2 + N_2 ambiance. This result indicates that O_2 played a key role in Hg^0 oxidization in the reactions. The highest Hg^0 removal efficiency was observed at 150 °C, with an efficiency of less than 35%. The Hg^0 removal efficiency was only 17% at 200 °C. It can also be inferred that physical adsorption probably dominated the Hg^0 removal reactions in the absence of O_2. Though Fe^{3+} and Cl^- have very strong oxidization abilities, their reactions with Hg^0 can only be activated and accelerated with the presence of O_2. The presence of O_2 in the feeding gas serves as a supplement for adsorbed oxygen and lattice oxygen in reactions, which is of significance for Hg^0 oxidization.

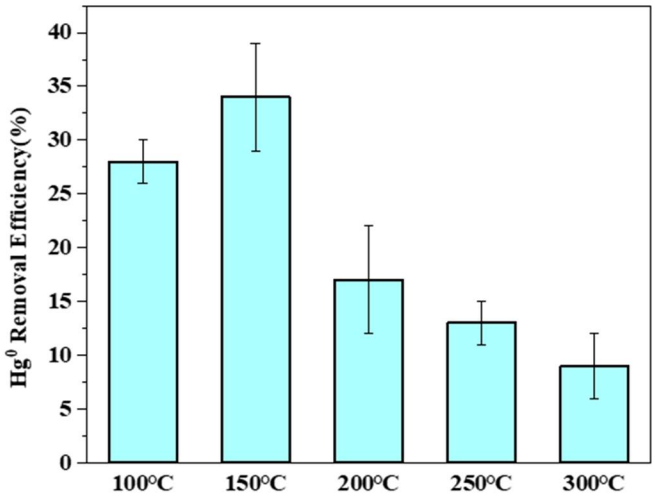

Figure 6. Hg^0 adsorption capabilities of MPTFC in N_2 ambiance.

3.4.5. Effects of Flue Gas Composition on the Hg^0 Removal Performance of MPTFC

In order to evaluate the impact of the flue gas components on Hg^0 adsorption of MPTFC, certain concentrations of NO and SO_2 were introduced into the reaction system in the experiments; the results are shown in Figure 7. It can be observed that the gas components had some impact on Hg^0 removal capability. Specifically, Hg^0 removal efficiency in N_2 was around 17%, whereas Hg^0 removal efficiency was boosted to around 95% when O_2 was introduced into the reaction system. When 200 ppm NO was added into the reaction system, Hg^0 removal efficiency increased to 98%. However, Hg^0 removal efficiency decreased to 71% when 500 ppm SO_2 was added into the reaction system, indicating the inhibiting effects of the SO_2 injection. When both NO and SO_2 were present in the reaction system, an improvement in Hg^0 adsorption capability was observed, and the Hg^0 removal efficiency increased to 87% in comparison with the SO_2-only ambiance. It can also be observed that an increase of NO in the flue gas from 200 ppm to 500 ppm inhibited Hg^0 adsorption capability slightly, which was probably due to competitive adsorption between NO and Hg^0 on the surface of the MPTFC. When NO was at a low concentration, the presence of NO promoted Hg^0 adsorption capability. This result was probably because the NO adsorbed on the surface formed NO_2 and NO, and those activated species reacted with Hg^0 to form HgO and Hg $(NO_3)_2$.

3.5. FTIR Measurements of MPTFC

Figure 8 shows the FTIR spectrums of PTFC, MPTFC, and spent MPTFC(S). It is evident that, after MPTFC was modified using $FeCl_3$ as a precursor, an obvious in-plane bending vibration of the C–H bond can be found at 1396 cm^{-1} in comparison with PTFC. In addition, the C–Cl bonding of MPTFC can also be found in the wavenumber of 686 cm^{-1}, indicating that Cl^- was successfully modified on the surface of PTFC. There is also a Fe–O characteristic peak showing in the wavenumber of 592 cm^{-1} for MPTFC(S), which is not identified for PTFC. This result indicates that the chemical reactions between $FeCl_3$ and PTFC occurred in the sample preparation. The presence of C–Cl and Fe–O in the sample indicates that $FeCl_3$ transformed into Cl-containing and Fe-containing active functional groups. Both of them contribute to Hg^0 adsorption. Further, it can also be observed that some of the carbon-containing functional groups disappeared after the Hg^0 adsorption reactions, indicating possible reactions between Hg^0 and those carbon-containing functional groups.

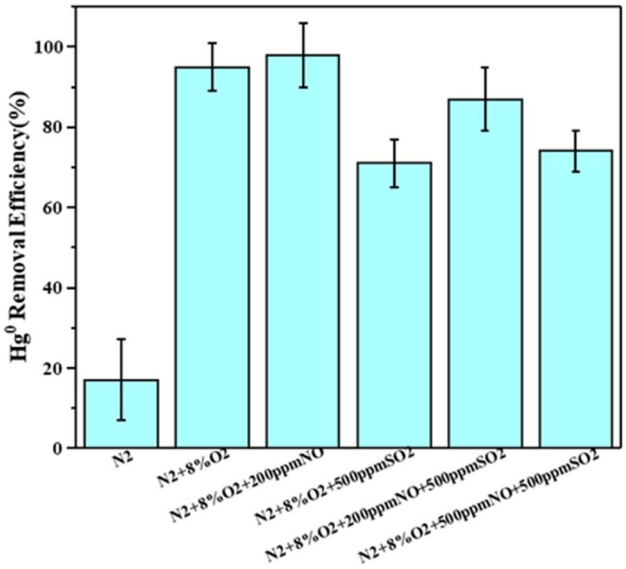

Figure 7. Gas component effects on the Hg^0 adsorption of MPTFC.

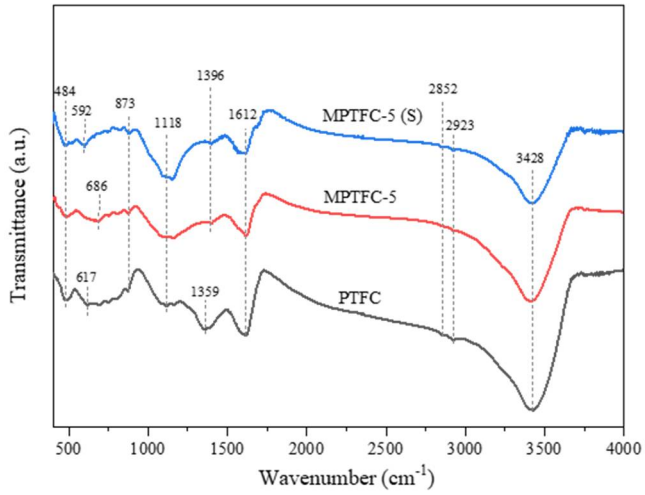

Figure 8. FTIR spectrums of PTFC, MPTFC, and MPTFC(S).

3.6. XPS Analysis of MPTFC before and after the Reactions

For a deep understating of the Hg^0 adsorption mechanisms of MPTFC, XPS analysis was adopted for the identified C 1s, O 1s, Cl 2p, Fe 2p, and Hg 4f spectrums for the sorbents before and after the reactions. The results are displayed in Figure 9. The C 1s spectrums for MPTFC before and after the Hg^0 adsorption experiments are shown in Figure 9a,b. Four major peaks can be observed, which are assigned as follows: C–C or C–H bonding at 284.3–284.8 eV, C–O or C–OH bonding at 284.9–285.6 eV, C–Cl bonding at 286.0–286.9 eV, and C=O bonding at 288.5–289.1 eV [32]. The relative contents of those C-bonding functional groups before and after the reactions are shown in Table 4. It can be observed that the content of the C–Cl and C=O functional groups decreased slightly after Hg^0 adsorption, while the contents of the C–O, C–C, and C–H functional groups increased after the reactions. This result indicates that C=O probably transformed into C–O or C–OH and further transformed into C–C or C–H groups. The decrease in C–Cl indicates that C–Cl was probably involved in the Hg^0 adsorption process in the reaction. These results are in accordance with the FTIR results.

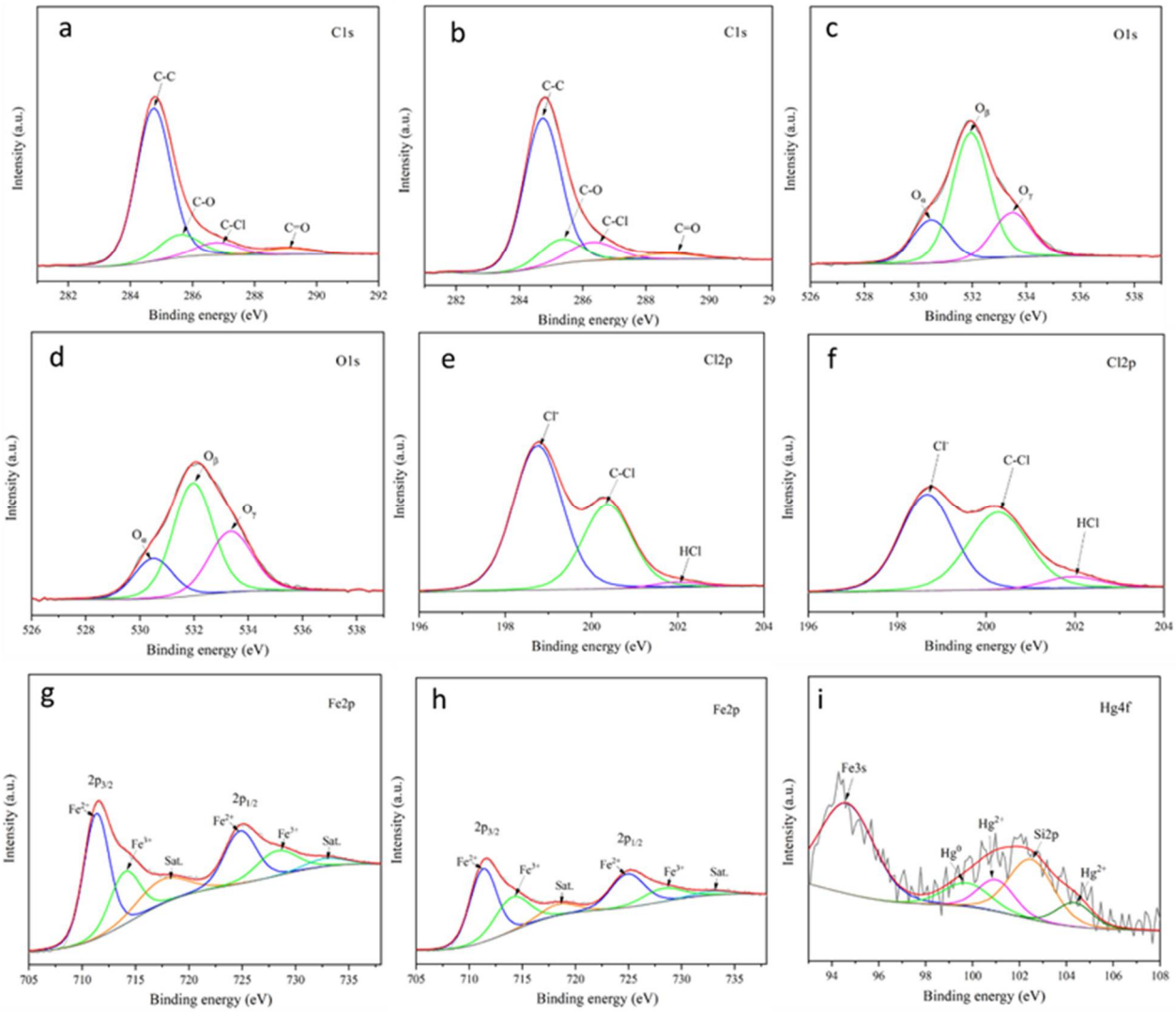

Figure 9. XPS spectrums of C 1s, O 1s, Cl 2p, Cl 2p, and Hg 4f of MPTFCs. (**a**,**b**) The C 1s spectrums for MPTFC before (**a**) and after (**b**) the Hg^0 adsorption experiments; (**c**,**d**) The O 1s spectrums for MPTFC before (**c**) and after (**d**) the Hg^0 adsorption experiments; (**e**,**f**) The Cl 2p spectrums before (**e**) and after (**f**) the reactions; (**g**,**h**) The Fe 2p spectrums of MPTFC before (**g**) and after (**h**) the reactions; (**i**) The Hg 4f spectrums for spent MPTFC.

Table 4. C-bonding functional groups before and after reactions on MPTFC.

Functional Groups	Before Reactions		After Reactions	
	Position (eV)	Content (%)	Position (eV)	Content (%)
C–C/C–H	284.75	70.70	284.73	74.71
C–O/C–OH	285.58	13.21	285.31	13.37
C–Cl	286.78	11.59	286.32	7.62
C=O	289.08	4.47	288.69	4.44

The O 1s spectrums for MPTFC before and after the Hg^0 adsorption experiments are shown in Figure 9c,d. It can be observed that lattice oxygen (O_α), adsorbed oxygen (O_β), and H_2O molecular oxygen (O_γ) can all be identified in the spectrums [33], which are assigned as 530.1–530.9 eV, 531.3–532.0 eV, and 532.6–533.5 eV, respectively. It can be observed that the content of O_α reduced from 20.9% to 17.29%, while O_β decreased from

87.83% to 51.15%. The consumption of O_α and O_β indicates that both were involved in the Hg^0 adsorption reactions [34].

The Cl 2p spectrums before and after the reactions are shown in Figure 9e,f. It can be observed that Cl^- and C–Cl are assigned as 198–198.9 eV and 199.6–200.4 eV, respectively [35]. The content of Cl^- increased from 48.98% to 61.84%, while the C–Cl content decreased from 44.76% to 36.65%. It can be inferred that, during the process of Hg^0 adsorption, C–Cl bonds were consumed, and Cl^- was produced in the reactions. Both XPS and FTIR confirmed that C–Cl was found to be involved in the Hg^0 adsorption reactions.

The Fe 2p spectrums of MPTFC before and after the reactions are shown in Figure 9g,h. The Fe^{2+} assigned to both 711.3–711.4 eV and 724.82 eV can be observed [36]. In addition, Fe^{3+} at 713.9–714 eV, 728.2–728.3 eV, and 732.7–732.8 eV can also be seen. Making a comparison between MPTFC before and after the reactions, it can be found that the content of Fe^{2+} increased from 54.24% to 57.93%, while that of Fe^{3+} decreased from 45.76% to 42.25%. This result indicates that Fe^{3+} was involved in Hg^0 removal during the experiment and then transformed to Fe^{2+}. The Fe-bearing oxides, probably Fe_2O_3 produced by $FeCl_3$ decomposition, may have provided lattice oxygen (Oα) that reacted with Hg^0 on the surface of the sorbent, thus forming the HgO- and Fe^{2+}-bearing oxides, such as FeO and Fe_3O_4 [37].

The Hg 4f spectrums for spent MPTFC are shown in Figure 9i. Several peaks can be observed. Characteristic peaks of Hg^{2+} can be observed at 101 eV and 104.35 eV [38], while Hg^0 can be found at 99.76 eV. The obvious peaks of Hg^{2+} confirm that Hg^0 was oxidized to form Hg^{2+}. The presence of Hg^0 is highly suspected to result from physical adsorption on the surface of MPTFC. The presence of Cl^- with Hg^{2+} is highly suspected to easily form Hg_2Cl_2 or $HgCl_2$. Both physical and chemical adsorptions occurred on MPTFC in the reactions. Several species, such as O_2, Fe^{3+}, and Cl^-, were great contributors to Hg^0 oxidation in the reactions.

4. Conclusions

An effective Hg^0 adsorbent, namely $FeCl_3$-modified phoenix tree fruit char (MPTFC), was developed using pyrolysis of phoenix tree fruit (PTF) combined with a $FeCl_3$ chemical immersion method. MPTFC was tested for Hg^0 adsorption capability in flue gas at different temperatures. Several analytical methods, specifically SEM, BET, EDS, FTIR, and XPS, were adopted to characterize the physicochemical properties of the sorbents. Phoenix tree fruit char (PTFC) presented as a tubular column micro-structure, which offered benefits for Hg^0 diffusion and adsorption. The $FeCl_3$ modification of PTFC only functionalized the surface of the sorbent without any alternations to the micro-structure of PTFC. Functional groups, such as C–Cl and Fe–O, were successfully decorated on the surface of PTFC after $FeCl_3$ modification. MPTFC exhibited an excellent Hg^0 adsorption capability of around 95% with 5% (wt.%) $FeCl_3$ modification at 200 °C in flue gas. O_2 was important for Hg^0 adsorption for MPTFCs. The presence of NO at a certain concentration also promoted Hg^0 removal efficiency, while SO_2 had negative impacts on Hg^0 adsorption. Functional groups, such as C–Cl and Fe–O, played a key role in Hg^0 adsorption, while C=O, lattice oxygen (O_α), and adsorbed oxygen (O_β) also contributed to Hg^0 adsorption and oxidization. Both the physical and chemical adsorption of Hg^0 on MPTFC occurred, and most of the Hg^0 on MPTFC probably oxidized to HgO and Hg_2Cl_2/$HgCl_2$.

Author Contributions: Conceptualization, C.T. and W.C.; methodology, Z.H., W.C. and M.L.; validation, C.T.; writing—original draft preparation, W.C.; writing—review and editing, C.T.; supervision, C.T. All authors have read and agreed to the published version of the manuscript.

Funding: This research was funded by the National Natural Science Foundation of China (Grant Nos. 52176127 and 51506066).

Institutional Review Board Statement: Not applicable.

Informed Consent Statement: Not applicable.

Data Availability Statement: Not applicable.

Acknowledgments: The authors gratefully acknowledge the financial support from the National Natural Science Foundation of China (Grant Nos. 52176127 and 51506066).

Conflicts of Interest: The authors declare no conflict of interest.

References

1. Li, H.; Zhu, L.; Wang, J.; Li, L.; Shih, K. Development of Nano-Sulfide Sorbent for Efficient Removal of Elemental Mercury from Coal Combustion Fuel Gas. *Environ. Sci. Technol.* **2016**, *50*, 9551–9557. [CrossRef] [PubMed]
2. Chen, L.; Liang, S.; Liu, M.; Yi, Y.; Mi, Z.; Zhang, Y.; Li, Y.; Qi, J.; Meng, J.; Tang, X.; et al. Trans-provincial health impacts of atmospheric mercury emissions in China. *Nat. Commun.* **2019**, *10*, 1–12. [CrossRef] [PubMed]
3. Xu, Y.; Luo, G.; Zhang, Q.; Li, Z.; Zhang, S.; Cui, W. Cost-effective sulfurized sorbents derived from one-step pyrolysis of wood and scrap tire for elemental mercury removal from flue gas. *Fuel* **2020**, *285*, 119221. [CrossRef]
4. Liu, H.; Chang, L.; Liu, W.; Xiong, Z.; Zhao, Y.; Zhang, J. Advances in mercury removal from coal-fired flue gas by mineral adsorbents. *Chem. Eng. J.* **2020**, *379*, 122263. [CrossRef]
5. Wu, Q.; Wang, S.; Liu, K.; Li, G.; Hao, J. Emission-Limit-Oriented Strategy To Control Atmospheric Mercury Emissions in Coal-Fired Power Plants toward the Implementation of the Minamata Convention. *Environ. Sci. Technol.* **2018**, *52*, 11087–11093. [CrossRef]
6. Yang, Y.; Liu, J.; Ding, J.; Yu, Y.; Zhang, J. Mercury/oxygen reaction mechanism over $CuFe_2O_4$ catalyst. *J. Hazard. Mater.* **2022**, *424*, 127556. [CrossRef]
7. Sasmaz, E.; Kirchofer, A.; Jew, A.D.; Saha, A.; Abram, D.; Jaramillo, T.F.; Wilcox, J. Mercury chemistry on brominated activated carbon. *Fuel* **2012**, *99*, 188–196. [CrossRef]
8. Wang, S.; Hao, J. Air quality management in China: Issues, challenges, and options. *J. Environ. Sci.* **2012**, *24*, 2–13. [CrossRef]
9. Yang, W.; Wang, Z.; Liu, Y. Review on Magnetic Adsorbents for Removal of Elemental Mercury from Flue Gas. *Energy Fuels* **2020**, *34*, 13473–13490. [CrossRef]
10. Zhao, S.; Pudasainee, D.; Duan, Y.; Gupta, R.; Liu, M.; Lu, J. A review on mercury in coal combustion process: Content and occurrence forms in coal, transformation, sampling methods, emission and control technologies. *Prog. Energy Combust. Sci.* **2019**, *73*, 26–64. [CrossRef]
11. Zhou, Q.; Tao, X.; Di, G.; Shang, Y.; Lu, P.; Xu, G.; Liu, M.; Zheng, Y.; Dong, L. SO_2 Tolerance and Mechanism of Elemental Mercury Removal from Flue Gas by a Magnetic Recyclable $Fe_6Mn_{0.8}Ce_{0.2}O_y$ Sorbent. *Energy Fuels* **2021**, *35*, 5101–5109. [CrossRef]
12. Li, H.; Zu, H.; Yang, Z.; Yang, J.; Xu, H.; Qu, W. The adsorption mechanisms of Hg_0 on marcasite-type metal selenides: The influences of metal-terminated site. *Chem. Eng. J.* **2021**, *406*, 126723. [CrossRef]
13. Yang, J.; Xu, H.; Zhao, Y.; Li, H.; Zhang, J. Mercury Removal from Flue Gas by Noncarbon Sorbents. *Energy Fuels* **2021**, *35*, 3581–3610. [CrossRef]
14. Wu, S.; Li, H.; Li, L.; Wu, C.-Y.; Zhang, J.; Shih, K. Effects of flue-gas parameters on low temperature NO reduction over a Cu-promoted CeO_2–TiO_2 catalyst. *Fuel* **2015**, *159*, 876–882. [CrossRef]
15. Zhang, J.; Duan, Y.; Zhou, Q.; Zhu, C.; She, M.; Ding, W. Adsorptive removal of gas-phase mercury by oxygen non-thermal plasma modified activated carbon. *Chem. Eng. J.* **2016**, *294*, 281–289. [CrossRef]
16. Zheng, J.-M.; Shah, K.J.; Zhou, J.-S.; Pan, S.-Y.; Chiang, P.-C. Impact of HCl and O_2 on removal of elemental mercury by heat-treated activated carbon: Integrated X-ray analysis. *Fuel Process. Technol.* **2017**, *167*, 11–17. [CrossRef]
17. Tang, R.; Yang, W.; Wang, H.; Zhou, J.; Zhang, Z.; Wu, S. Preparation of Fly-Ash-Modified Bamboo-Shell Carbon Black and Its Mercury Removal Performance in Simulated Flue Gases. *Energy Fuels* **2016**, *30*, 4191–4196. [CrossRef]
18. Yang, J.; Zhao, Y.; Zhang, J.; Zheng, C. Removal of elemental mercury from flue gas by recyclable $CuCl_2$ modified magnetospheres catalyst from fly ash. Part 1. Catalyst characterization and performance evaluation. *Fuel* **2016**, *164*, 419–428. [CrossRef]
19. Yang, W.; Chen, H.; Han, X.; Ding, S.; Shan, Y.; Liu, Y. Preparation of magnetic Co-Fe modified porous carbon from agricultural wastes by microwave and steam activation for mercury removal. *J. Hazard. Mater.* **2020**, *381*, 120981. [CrossRef]
20. Li, H.; Feng, S.; Yang, Z.; Yang, J.; Liu, S.; Hu, Y.; Zhong, L.; Qu, W. Density Functional Theory Study of Mercury Adsorption on CuS Surface: Effect of Typical Flue Gas Components. *Energy Fuels* **2019**, *33*, 1540–1546. [CrossRef]
21. Zhang, X.; Duan, Y.; Wang, H.; Ren, S.; Wei, H. Effect of flue gas components on Hg^0 oxidation and adsorption by modified walnut shell coke in O_2/CO_2 atmosphere. *Asia-Pac. J. Chem. Eng.* **2020**, *15*, e2423. [CrossRef]
22. Gao, L.; Li, C.; Zhang, J.; Du, X.; Li, S.; Zeng, J.; Yi, Y.; Zeng, G. Simultaneous removal of NO and Hg^0 from simulated flue gas over CoOx-CeO_2 loaded biomass activated carbon derived from maize straw at low temperatures. *Chem. Eng. J.* **2018**, *342*, 339–349. [CrossRef]
23. Shan, Y.; Yang, W.; Li, Y.; Liu, Y.; Pan, J. Preparation of microwave-activated magnetic bio-char adsorbent and study on removal of elemental mercury from flue gas. *Sci. Total Environ.* **2019**, *697*, 134049. [CrossRef]
24. Yang, W.; Liu, Z.; Xu, W.; Liu, Y. Removal of elemental mercury from flue gas using sargassum chars modified by NH4Br reagent. *Fuel* **2018**, *214*, 196–206. [CrossRef]
25. Shen, B.; Tian, L.; Li, F.; Zhang, X.; Xu, H.; Singh, S. Elemental mercury removal by the modified bio-char from waste tea. *Fuel* **2017**, *187*, 189–196. [CrossRef]

26. Yang, W.; Liu, Y.; Pan, J. Experimental and kinetic study on Hg^0 removal by microwave/hydrogen peroxide modified seaweed-based porous biochars. *Environ. Technol. Innov.* **2021**, *22*, 101411. [CrossRef]
27. Altaf, A.R.; Teng, H.; Zheng, M.; Ashraf, I.; Arsalan, M.; Rehman, A.U.; Gang, L.; Pengjie, W.; Ren, Y.; Lu, X. One-step synthesis of renewable magnetic tea-biochar derived from waste tea leaves for the removal of Hg^0 from coal-syngas. *J. Environ. Chem. Eng.* **2021**, *9*, 105313. [CrossRef]
28. Li, Y.; Liu, Y.; Yang, W.; Liu, L.; Pan, J. Adsorption of elemental mercury in flue gas using biomass porous carbons modified by microwave/hydrogen peroxide. *Fuel* **2021**, *291*, 120152. [CrossRef]
29. Shen, B.; Liu, Z.; Xu, H.; Wang, F. Enhancing the absorption of elemental mercury using hydrogen peroxide modified bamboo carbons. *Fuel* **2019**, *235*, 878–885. [CrossRef]
30. Lee, S.J.; Seo, Y.-C.; Jurng, J.; Lee, T.G. Removal of gas-phase elemental mercury by iodine- and chlorine-impregnated activated carbons. *Atmos. Environ.* **2004**, *38*, 4887–4893. [CrossRef]
31. Cai, J.; Shen, B.; Li, Z.; Chen, J.; He, C. Removal of elemental mercury by clays impregnated with KI and KBr. *Chem. Eng. J.* **2014**, *241*, 19–27. [CrossRef]
32. Tan, Z.; Niu, G.; Chen, X. Removal of elemental mercury by modified bamboo carbon. *Chin. J. Chem. Eng.* **2015**, *23*, 1875–1880. [CrossRef]
33. Xu, W.; Adewuyi, Y.G.; Liu, Y.; Wang, Y. Removal of elemental mercury from flue gas using CuOx and CeO_2 modified rice straw chars enhanced by ultrasound. *Fuel Process. Technol.* **2018**, *170*, 21–311. [CrossRef]
34. Xie, Y.; Li, C.; Zhao, L.; Zhang, J.; Zeng, G.; Zhang, X.; Zhang, W.; Tao, S. Experimental study on Hg^0 removal from flue gas over columnar MnO_x-CeO_2/activated coke. *Appl. Surf. Sci.* **2015**, *333*, 59–67. [CrossRef]
35. Li, G.; Wu, Q.; Wang, S.; Li, Z.; Liang, H.; Tang, Y.; Zhao, M.; Chen, L.; Liu, K.; Wang, F. The influence of flue gas components and activated carbon injection on mercury capture of municipal solid waste incineration in China. *Chem. Eng. J.* **2017**, *326*, 561–569. [CrossRef]
36. Han, L.; He, X.; Yue, C.; Hu, Y.; Li, L.; Chang, L.; Wang, H.; Wang, J. Fe doping Pd/AC sorbent efficiently improving the Hg^0 removal from the coal-derived fuel gas. *Fuel* **2016**, *182*, 64–72. [CrossRef]
37. Liu, D.; Xu, W.; Liu, Y. Seaweed bio-chars modified with metal chloride for elemental mercury capture from simulated flue gas. *Atmos. Pollut. Res.* **2020**, *11*, 122–130. [CrossRef]
38. Zhao, L.; Li, C.; Zhang, J.; Zhang, X.; Zhan, F.; Ma, J.; Xie, Y.; Zeng, G. Promotional effect of CeO_2 modified support on V_2O_5–WO_3/TiO_2 catalyst for elemental mercury oxidation in simulated coal-fired flue gas. *Fuel* **2015**, *153*, 361–369. [CrossRef]